EDGE ARTICLE

Check for updates

Influence of H⁺, OH⁻ and salts on hydrophobic self-assembly†

Kenneth D. Judd,‡ Denilson Mendes de Oliveira, [ID] ‡ Andres S. Urbina [ID] and Dor Ben-Amotz [ID] *

In spite of the ubiquity of acid/base ions and salts in biological systems, their influence on hydrophobic self-assembly remains an open question. Here we use a combined experimental and theoretical strategy to quantify the influence of H^+ and OH^-, as well as salts containing Li^+, Na^+, Cl^- and Br^-, on the hydrophobic self-assembly of micelles composed of neutral oily 1,2-hexanediol surfactants. The distributions of aggregate sizes, both below and above the critical micelle concentration (CMC), are determined using Raman multivariate curve resolution (Raman-MCR) spectroscopy to quantify the multi-aggregation chemical potential surface (MCPS) that drives self-assembly. The results reveal that ions have little influence on the formation of hydrophobic contact dimers but can significantly drive high-order self assembly. Moreover, the hydration-shells of oily solutes are found to expel the above salt ions and OH^-, but to attract H^+, with wide-ranging implications.

1. Introduction

Oily molecules and salty water are ubiquitous accomplices in biological and synthetic self-assembly, including the formation of cell membranes, micelles and host–guest complexes as well as protein and polymer folding.[1–9] Although most ions "salt-out" oily molecules (by lowering their solubility), and thus might be expected to promote hydrophobic self-assembly, quantifying and predictively understanding the influence of ions on the formation of hydrophobic aggregate structures of different sizes remains an outstanding challenge. This is particularly true with regard to the influence of acid–base ions, H^+ and OH^-, on the formation of both low-order contact dimers and high-order aggregates, such as the self-assembly of micelles above the corresponding critical micelle concentration (CMC), as well as open questions regarding the affinity of these ions for air–water and oil–water interfaces.[10–13] Here we address these questions by combining Raman multivariate curve resolution (Raman-MCR) spectroscopy and a multi-aggregation chemical potential surface (MCPS) analysis strategy[14] applied to 1,2-hexanediol (12HD) micelle formation.[14–16] This neutral oily surfactant is ideally suited to quantifying the influence of ions on hydrophobic self-assembly as 12HD does not chemically react with acids, bases or salts and is not influenced by competing

electrostatic and ion-exchange contributions that may affect the self-assembly of ionic micelle forming surfactants.[17–19] Our results reveal that H^+ and OH^- have dramatically different effects on both the solubility and CMC of 12HD, implying that the oily hydration-shell of 12HD expels OH^- but attracts H^+, thus contributing to the resolution of open questions regarding the charge and ion affinity of oily interfaces.[8,10,13,20,21] Moreover, our results indicate that while salting-out ions such as Na^+, Cl^- and OH^- significantly stabilize higher-order aggregates and micelles, they have a negligible influence on binary hydrophobic contact free energies and dimerization equilibria, for reasons revealed by the present analysis, with broader implications to other hydrophobic self-assembly processes.

The salting-out strengths of many ions have been determined from measurements of the solubilities of non-polar gases such as H_2 and O_2,[22] and molecular oily solutes including linear alkanes[23,24] and alcohols,[25–27] as well as benzene and many other solutes.[22,28] Although relatively few prior measurements pertain to H^+ and OH^-, benzene solubility measurements in aqueous NaOH and HCl suggest that OH^- is more strongly salting-out than H^+.[22] It has also long been recognized that while the salting-out strength of monovalent anions increases with decreasing anion size, cations have a non-monotonic size dependence, as Na^+ is more strongly salting-out than both smaller and larger alkali cations (such as Li^+ and Cs^+).[22,29,30] The predictive understanding of these anion and cation size dependent trends has been significantly advanced by recent simulation studies,[29,30] including simulations of both the solubility and dimerization of methane in aqueous ionic solutions,[29,31] although these simulations did not extend to higher-order aggregates, or include H^+ and OH^- ions.

Department of Chemistry, Purdue University, West Lafayette, IN 47907, USA. E-mail: dorbenamotz@gmail.com

‡ These authors contributed equally as co-first-authors.

Prior studies of the influence of aqueous ions on 12HD micelle formation include fluorescent probe measurements combined with a scaled particle theory based analysis, assuming that ions only influence the solvation free energy of the free monomers.[15] A subsequent probe-free Raman-MCR based study obtained similar ion-induced CMC shifts, but the associated Wyman–Tanford analysis suggested that ions may influence the solubilities of both the free and micelle-bound 12HD molecules.[16] The present combined experimental and theoretical results are the first to quantify the influence of ions on both the free and micelle-bound 12HD molecules, as well as the first to include H^+ and OH^-, thus revealing that salting-out ions lower the solubility of free 12HD about twice as much as micelle-bound 12HD, with the exception of H^+ whose affinity for 12HD nearly perfectly cancels the salting-out effect of a Cl^- counter-ion. Moreover, the results yield the first quantitative measures of the influence of ions on aggregate size distributions, revealing that ions have little influence on low-order pre-micellar aggregate distributions but may significantly promote the onset of high-order aggregation.

2. Analysis strategy

Prior studies have demonstrated the utility of Raman-MCR as a probe-free experimental method for quantifying micelle formation, hydration and solubilization.[14,16,32,33] Here Raman-MCR C–H band shape and intensity changes are used to quantify MCPS aggregate size distributions[14] and solubilities.[11] Briefly, the equilibrium between free solute monomers and aggregates of size n may be expressed as

$$C_n/C_A = (C_1/C_A)^n \tag{1}$$

where C_n is the total (equilibrium) concentration of solutes that are contained in aggregates of size n, and thus C_1 is the equilibrium concentration of free (unbound) solutes.[14] The n-dependent critical aggregation concentration

$$C_A = \left[\left(\frac{1}{n}\right) e^{\beta n \Delta \mu_n^0} \right]^{\frac{1}{n-1}} \tag{2}$$

is equivalent to the value of C_1 at which $C_1 = C_n$, which is a function of the MCPS, $\Delta \mu_n^0$, defined as the n-dependent difference between the chemical potentials of the bound and free solutes

$$\Delta \mu_n^0 = \mu_n^0 - \mu_1^0 \tag{3}$$

where $\beta = 1/RT$, R is the molar Boltzmann constant and T is the absolute temperature. The chemical potentials μ_n^0 pertain to solute molecules contained in aggregates of size n at a 1 M standard state concentration (of the solutes, not the aggregates). Eqn (1) and (2) assume that the aggregates do not significantly interact with each other at solute concentrations up to 1 M (note that the concentration of aggregates is $1/n$ times the corresponding solute concentration). Thus, eqn (1) and (2) are equivalent to the usual relation between an n-fold aggregation equilibrium constant $K_n \equiv [n]/[1]^{n-1}$ (where $[n]$ is the

concentration of aggregates of size n) and the corresponding standard state free energy difference $\Delta G_n^0 = n\Delta\mu_n^0 = -RT \ln K_n$ (as further described in the ESI, Theoretical methods Section†).

It has recently been demonstrated that micelle formation is well described by assuming that the MCPS is a quadratic function of n,[14] thus motivating our use of this approximation in the present analyses. The quadratic MCPS has a minimum value of $\Delta\mu_{n*}^0$ at $n = n^*$, which determines the value of $C_A(n^*)$, and thus the experimental CMC, as well as the characteristic micelle size, whose aggregate size distribution peaks near n^*. The values of the two MCPS parameters, $\Delta\mu_{n*}^0$ and n^*, also determine the width of the aggregate size distribution, dictated by the curvature of the quadratic $\Delta\mu_n^0$ function. The latter n-dependent function is assumed to continuously extend down to $n = 1$ (at which $\Delta\mu_1^0 = 0$), in keeping with the expectation that the value of $\Delta\mu_n^0$ cannot differ much from its values at $n \pm 1$.[14] The only other adjustable parameter in the MCPS model is n_L, which determines the range of aggregate sizes that are included in the pre-micellar low-order aggregate size distribution (as further explained below).[14] As we will see, the values of $\Delta\mu_{n*}^0$ and CMC can be more accurately determined than the values of n^* and n_L, but the uncertainties of the latter two parameters do not significantly influence the resulting CMC and its ion-sensitivity, or any of the primary conclusions of this work.

MCPS predictions are linked to experimental Raman-MCR measurements by equating the 12HD free monomer fraction and C–H frequency shift $C_f/C_T = (\langle\omega\rangle - \omega_m)/(\omega_f - \omega_m)$, where C_f and $C_T = \sum_n C_n$ are free and total solute concentrations, $\langle\omega\rangle$ is the measured average C–H frequency at a given solute concentration, and ω_f and ω_m are the limiting free and micelle-bound average C–H frequencies, respectively. The free monomer fraction may also be determined by decomposing the measured C–H bandshape into a linear combination of free and micelle-bound C–H band shapes[14] (as described in the Methods summary and ESI†). Since pre-micellar low-order aggregates may contribute to the measured C–H spectrum at concentrations below CMC, the experimentally determined C_f is an effective free monomer concentration that includes contributions from low-order aggregates. Thus, the spectra arising from aggregates with $1 < n \leq n_L$ are treated as partially free, in proportion to the fractional aggregation state of the surfactant.[14]

$$C_f = \sum_{n=1}^{n_L} \left(\frac{n_L + 1 - n}{n_L}\right) C_n \tag{4}$$

The corresponding 12HD micelle-bound solute concentration is $C_m = C_T - C_f$ and thus $C_f/C_T = 1 - C_m/C_T$. The experimental CMC is equated with the value of C_f at which $C_f = C_m$ (which occurs when $C_T = 2$CMC).[14] The above connection between MCPS predictions and Raman-MCR measurements relies on the experimental observation that 12HD spectra in pure water and aqueous ionic solutions of 12HD may be accurately decomposed into a linear combination of free and micelle-bound spectral components[14] (as further explained in the ESI†).

The chemical potential of a solute $\mu_{n,s}^0$ in an aqueous solution with a salt (counter-ion pair) concentration of C_s may be expressed as

$$\mu_{n,s}^0 = \mu_n^0 + k_n C_s \tag{5}$$

where

$$k_n = \frac{RT}{C_s}\ln\left(\frac{S_0}{S}\right) = \frac{RT}{C_s}\ln\left(\frac{P}{P_0}\right) \tag{6}$$

is determined either from the solubility (S) or n-octanol/water partition coefficient (P) of the solute in the salt solution, relative to pure water (S_0 or P_0).

The influence of ions on the MCPS may thus be expressed as

$$\Delta\mu_{n,s}^0 = \Delta\mu_n^0 + \Delta k_s C_s \tag{7}$$

where $\Delta\mu_{n,s}^0 = \mu_{n,s}^0 - \mu_{n,1}^0$ and $\Delta k_s = k_n - k_1$. The resulting experimental CMC and MCPS parameters are obtained as above, with the MCPS equal to $\Delta\mu_{n,s}^0$ rather than $\Delta\mu_n^0$ (as further described in the Methods summary and ESI†). The coefficients k_n may also be described using Kirkwood–Buff and Wyman–Tanford theories,[11,16,29] revealing that the sign and magnitude of k_n is linked to the degree of expulsion ($k_n > 0$) or accumulation ($k_n < 0$) of ions in the solute's hydration-shell. Note that both $\mu_{n,s}^0$ and $\Delta\mu_{n,s}^0$ are typically nearly linear functions of C_s up to molar salt concentrations,[15,22] and thus both k_n and Δk_s are typically constant (independent of salt concentration) up to salt concentrations of $\gtrsim 2$ M.

3.   Results and discussion

Fig. 1 shows experimental Raman-MCR and MCPS results pertaining to the aggregation of 12HD in pure water. The green solute-correlated (SC) spectrum in Fig. 1(a) contains vibrational features arising from the solute and its hydration-shell. The largest band in this SC spectrum is the C–H stretch band of 12HD, whose mean frequency shift is used to quantify the aggregation of 12HD. The C–H band is decomposed into pre-micelle (free) and micellar components, indicated by the dashed and dotted curves in Fig. 1(b), obtained from MCPS fits to the experimental C–H bands as previously described[14] (see Methods summary and ESI† for further details).

The dotted and dashed colored curves in Fig. 1(c) illustrate the nearly equally good fits obtained with $35 \leq n^* \leq 100$ and $7 \leq n_L \leq 20$, although the resulting values of CMC = 0.69 ± 0.03 (as well as $\Delta\mu_{n^*}^0/RT = 1 \pm 0.1$ and $C_A(n^*) = 0.35 \pm 0.15$) are relatively insensitive to the uncertainties of n^* and n_L. Fig. 1(d) shows the resulting concentrations of the pre-micellar and micellar sub-populations, as well as an inset panel showing the resulting experimentally derived $\beta\Delta\mu_n^0$. Fig. 1(e) shows how the predicted aggregate size distributions depend on the total concentration of 12HD, C_T, leading to the emergence of the micellar high-order aggregate population when C_T exceeds CMC ~0.7 M. The inset panel in Fig. 1(e) reveals that below CMC the nearly exponentially n-dependent low-order aggregate size distributions broaden with increasing concentration, and then
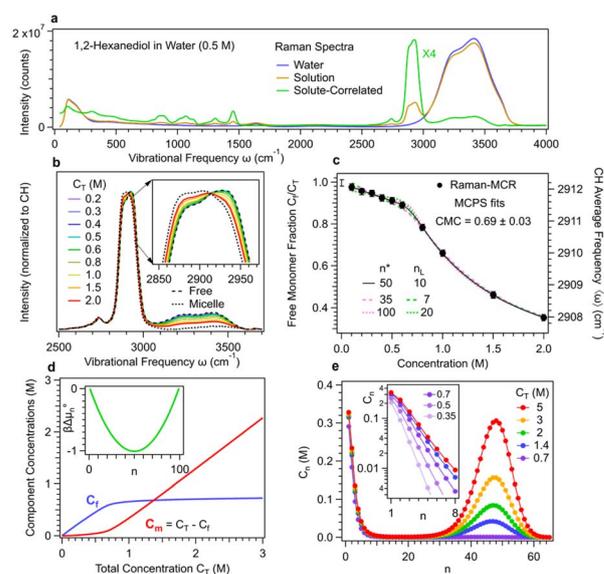

Fig. 1 Experimental Raman-MCR spectra and MCPS fit predictions for the aggregation of 12HD in pure water. (a) Raman spectra and Raman-MCR SC spectra. (b) Concentration dependence of the SC spectra, with the inset panel highlighting the change in the C–H band, and the dashed and dotted curves representing the limiting free monomer and pure micelle spectra. (c) Fraction of free (non-micellar) 12HD molecules, and average C–H frequency, plotted as function of 12HD concentration. (d) The apparent free (C_f) and micelle (C_m) concentrations, with an inset panel showing the quadratic chemical potential surface $\beta\Delta\mu_n^0 = \Delta\mu_n^0/RT$. (e) Concentration dependence of the aggregate size distribution below and above CMC ~0.69 M.

become nearly concentration-independent after the emergence of high-order micellar aggregates (when $C_T > 2$ CMC).

Fig. 2 shows experimental Raman-MCR and MCPS fits revealing the influence of ions on 12HD micelle formation. Fig. 2(a) compares experimental (points) and MCPS fits (curves) pertaining to the free monomer fraction C_f of 12HD in pure water and 2 M solutions of three alkali-halide salts (NaBr, LiCl and NaCl). The blue points in Fig. 2(a) show the excellent agreement between results obtained using a high ($\times$, 1200 g mm^{-1}) and low ($+$, 300 g mm^{-1}) resolution Raman spectrometer diffraction gratings, and all the remaining results were obtained using the low-resolution grating. Fig. 2(b) shows the corresponding results in 2 M solutions of two acids (HCl and HBr) and two bases (LiOH and NaOH) along with the pure water (dotted blue) and 2 M NaCl (dashed black) results. The CMC values shown in Fig. 1(a) and (b) are obtained from MCPS fits with $n^* = 50$ and $n_L = 10$. The relative insensitivity of the MCPS fits to the assumed value of n^* makes it impossible to reliably determine whether ions significantly influence micelle size, although one might expect more strongly salting-out ions to shift the micelle size distribution to larger n (and salting-in ions to favor the formation of smaller micelles).

Fig. 2(c) and (d) compare MCPS C_f and ΔG predictions, respectively, spanning the experimentally relevant range of CMC = 0.3, 0.5, and 0.7 M. Note that ΔG pertains to the total free energy of micellization, obtained by treating the system as an effective two-component mixture of free and micelle-bound
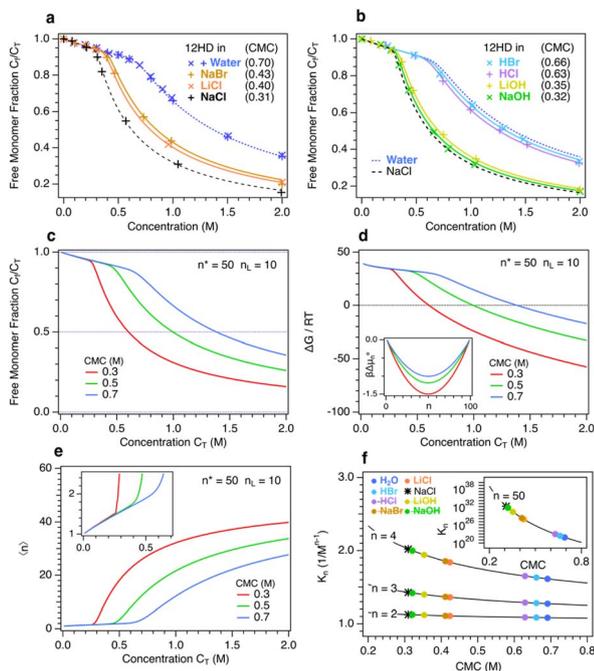
Fig. 2 Influence of ions on 12HD micelle formation. (a) and (b) show the free monomer fraction in pure water and various 2 M counter-ion solutions. The MCPS fit curves in (a) and (b) were obtained assuming $n^* = 50$ and $n_L = 10$ and the resulting CMC values are given in the legend (in parentheses). The MCPS predictions in (c) and (d) pertaining to CMC = 0.3, 0.5, and 0.7 M, spanning the experimental range, with the corresponding quadratic MCPS, $\beta\Delta\mu_n^0$, curves shown in the (d) inset panel. (e) and (f) show the average aggregation number $\langle n \rangle$ and equilibrium constant K_n predictions, respectively, with colored points in (f) corresponding to predictions obtained from MCPS fits to the experimental results.

solutes (as further explained in the ESI†). The micelle formation ΔG predictions reveal that at low concentration an equimolar mixture of free monomers and micelles is ~40 kJ mol^{-1} higher in free energy than a free monomer solution, while at high concentrations the equimolar mixture is strongly driven to form a predominantly micellar solution. Note that the concentrations at which $C_f/C_T = 0.5$ (and thus $C_f/C_m = 1$) in Fig. 2(c) are the same as the concentrations at which $\Delta G = 0$ in Fig. 2(d), whose inset panel shows the corresponding MCPS, $\beta\Delta\mu_n^0$.

Fig. 2(e) shows MCPS predictions of the 12HD concentration dependence of the average aggregation size $\langle n \rangle = \sum n \, C_n / \sum C_n$. Note that below CMC $\langle n \rangle < 2$, indicating that at low concentrations the aggregate size distribution consists primarily of monomers and dimers, and is insensitive to the value of CMC, because $\beta\Delta\mu_2^0$ is invariably much smaller than 1 and thus dimers result from random mixing contacts (as further explained below). Fig. 2(f) shows the corresponding equilibrium constant K_n predictions as a function of CMC for various n-fold aggregation equilibria, with colored points pertaining to the experimentally derived results in various 2 M aqueous ionic solutions. Note that the dimerization equilibrium constant K_2 predictions shown in Fig. 2(f) are remarkably ion-insensitive, while the higher order aggregation equilibrium constants become more ion-sensitive with increasing aggregate

size. The ion-insensitivity of dimerization equilibria results from the fact that $|\Delta\mu_2^0| \ll RT$, required by the physical constraint that the MCPS must be a smooth function of n down to $n = 1$, combined with fact that $|\Delta\mu_{n*}^0| \sim RT$. In other words, the value of $\Delta\mu_2^0$ must be much smaller than $\Delta\mu_{n*}^0$ since solutes contained in a dimer are necessarily in a less oily environment than those contained in a micelle. Thus, the experimental observation that $|\Delta\mu_{n*}^0| \sim RT$ requires that $|\Delta\mu_2^0| \ll RT$. The latter conclusion is not necessarily incompatible with a more significant influence of ions on the corresponding osmotic second virial coefficient B,[31] since $\Delta\mu_2^0$ is an effective contact free energy while B may be influenced by correlations at length scales well beyond direct contact.

Since dimer contact free energies are invariably much smaller than thermal energy, dimer contact probabilities are essentially random in both pure water and 2 M salt (as well as acid and base) solutions. However, the ion-insensitivity of K_2 does not imply that the monomer and dimer solubilities are ion-insensitive, but rather that ions have a very similar influence on the chemical potentials of both the free and dimer-bound 12HD molecules. In other words, the ion-insensitivity of dimerization equilibria is consistent with the expectation that the dimers remain nearly fully hydrated and thus are nearly as strongly salted-out as a pair of free monomers. In higher order aggregates, on the other hand, the 12HD molecules are increasingly shielded from the solvent, thus reducing their ion-induced salting-out and stabilizing them relative to the more strongly salted-out free monomers. Although the micelle-bound 12HD molecules are substantially shielded from the solvent, the following results reveal that ions nevertheless have a substantial influence on the solubility of the high-order aggregates, and thus the ion-induced shift in CMC is significantly smaller than it would be if the micelle solubility was ion-independent.

Fig. 3 compares the influence of various ions on the solubility of both free and micelle-bound oily molecules. The upper two panels in Fig. 3 show experimental ion-induced changes in the solubility of various n-alkane[23,24] and n-alcohol[25,26] solutes,[34] as well as benzene,[22] including our measurements of the solubilities of 1-hexanol and 12HD. These results indicate that increasing the size or chain length of an oily molecule generally increases the ion-sensitivity of its solubility. The fact that sodium chloride (NaCl) salts-out n-alkanes more strongly than lithium chloride (LiCl) is consistent with the previously noted non-monotonic cation size dependence, with a salting-out maximum for Na$^+$.[22,28,29] This cation size dependent trend clearly continues with H$^+$, as HCl is more weakly salting out than LiCl. The same trend holds for benzene, now with the inclusion of NaOH, which is slightly more strongly salting out than NaCl, thus indicating that the OH$^-$ is slightly more expelled from the hydration-shell of benzene than is Cl$^-$. These general trends carry over to the n-alcohols results shown in Fig. 3(b), revealing a decrease in salting-out with decreasing cation size, as well as the strong salting-out strength of OH$^-$. The 12HD points in Fig. 3(b) show a similar trend, but with a lower cation-size dependent variation and similar salting-out
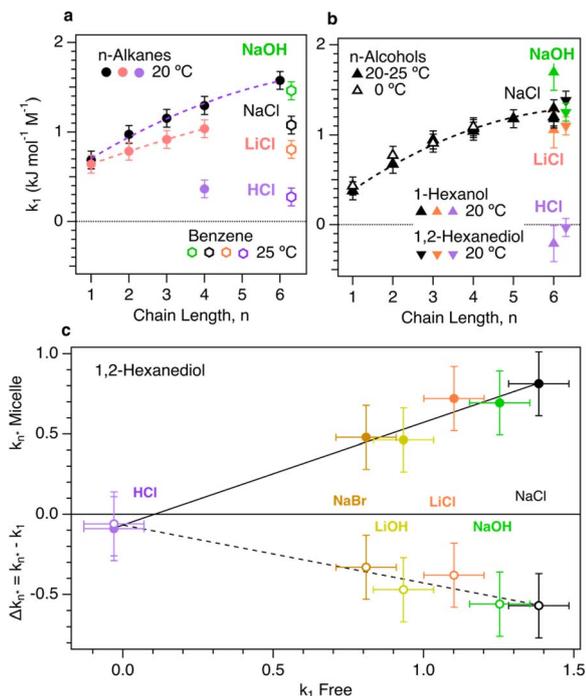
Fig. 3 Influence of ions on the solubility of alkanes, alcohols and both free and micelle-bound 12HD. (a) Normal alkanes up to n-hexane[23,24] and benzene.[22] (b) Normal alcohols up to n-hexanol[25–27] including the present Raman-MCR based results for n-hexanol and 12HD. (c) Raman-MCR/MCPS based measurements of 12HD Δk_{n*} are plotted as a function of k_1 and used to obtain the corresponding micelle solubility coefficients k_{n*}.

behavior of NaCl and NaOH. Comparisons of the results in Fig. 3(a) and (b) further reveal that the salting-out coefficients of n-alcohols are nearly identical to those of the corresponding n-alkanes with one-fewer carbon atoms. This suggests that the methylene (CH_2) group associated with alcohol OH head group is not as influenced by ions as the remaining non-polar CH_2 and CH_3 groups. Moreover, the same trend appears to carry over to 12HD, which is salted-out by almost the same amount as the n-alkanes with two-fewer carbon atoms, again suggesting the two OH-bound CH_2 groups are not significantly influenced by the dissolved ions.

The lower panel in Fig. 3 compares the salting-out coefficients of micelle-bound 12HD molecules, k_{n*} (obtained from the experimental k_1 and $\Delta k_{n*} = k_{n*} - k_1$) plotted as a function of the unbound 12HD salting-out coefficient, k_1. Note that in 2 M NaCl solutions the k_{n*} salting-out coefficient for micelle-bound 12HD is about 40% smaller than that of the free monomers, k_1, and approximately the same is true for other salting-out ion-pairs. This indicates that NaCl (like other salting-out ion-pairs) significantly decreases the solvation free energy of both the free and micelle-bound 12HD molecules, implying that the micelle-bound oily chains of 12HD remain significantly exposed to both water and ions. As a result, the shift in CMC is significantly smaller than it would be if the ions only influenced the solubility of the free monomers. The linear correlation between k_{n*} and k_1 is consistent with the linear dependence of both $\mu_{n,s}^0$ and $\mu_{1,s}^0$ on salt concentration, with a slope that increases

with the degree to which the oily solute chains are exposed to the aqueous ionic solvent.

The difference between the influence of OH^- and H^+ on hydrophobic aggregation is clearly evidenced by the results shown in Fig. 3. Note that NaCl and NaOH (as well as LiCl and LiOH) produce a similar decrease in CMC (and also a similar decrease in the solubilities of alkanes and alcohols). Since various lines of experimental and theoretical evidence indicate that both OH^- and Cl^- are salting-out ions,[11,28] the present results imply that Cl^- and OH^- are both similarly expelled from oily hydration-shells. On the other hand, the nearly neutral influence of HCl on both CMC and the solubilities of alkanes and alcohols implies that H^+ increases the solubility of 12HD to a degree that nearly cancels the salting-out effect of Cl^-, thus implying that H^+ is attracted rather than expelled from the hydration-shells of oily molecules. Although the reason for this remarkable behavior of H^+ remains an open question, it may be influenced by the electrostatic attraction of H^+ to the negative charge at oil–water interfaces, as inferred from recent experimental and theoretical results.[10,20,21] If so, then the present results imply that a similar negative charge accumulates at molecular oily surfaces, thus potentially influencing a wide range of biological and synthetic hydrophobic folding, binding, and assembly processes. Note that any such electrostatic contribution to the affinity of cations for oily interfaces should be greatest for H^+ as compared to larger (lower charge density) cations.

4. Methods summary

Raman spectra of aqueous solutions containing 12HD in either pure water or water containing 2 M salt (or ion-pairs) were measured using a home built spectrometer and self-modelling curve resolution (SMCR) was used to obtain solute-correlated (SC) spectra from pairs of solvent and 12HD solution spectra, as previously described.[14,16] The resulting C–H average frequencies of the free (ω_f) and micelle-bond (ω_m) species were determined either by extrapolation of the MCPS fits to low and high concentration, or from the corresponding limiting spectra obtained using a hybrid Raman-MCR/MCPS spectra decomposition strategy described in the appendix of ref. 14. The influence of ions on the solubility coefficients, k_s, of 12HD were quantified by measuring the integrated area of the C–H band in equilibrated two-phase solutions created using either pure water or an aqueous counter-ion solution, as previously described.[11] Further details regarding the experimental and theoretical methods are provided in the ESI Methods.†

Data availability

Archived experimental data and analysis procedures are available in the Purdue University Research Repository, DOI: **10.4231/8GBW-9P30**.

Author contributions

The co-first authors Kenneth D. Judd and Denilson Mendes de Oliveira performed most of the experimental measurements

and contributed to writing the manuscript. Andres S. Urbina performed and refined solubility measurements and contributed to writing the manuscript. Dor Ben-Amotz directed the research, performed the MCPS analyses, and contributed to writing the manuscript.

Conflicts of interest

There are no conflicts to declare.

Acknowledgements

References

1 W. Kauzmann, Some Factors in the Interpretation of Protein Denaturation, *Adv. Protein Chem.*, 1959, **14**, 1–63.

2 C. Tanford, *The Hydrophobic Effect: Formation of Micelles and Biological Membranes*, Wiley, New York, 2nd edn, 1980.

3 D. Chandler, Interfaces and the Driving Force of Hydrophobic Assembly, *Nature*, 2005, **437**, 640–647.

4 P. Ball, Water as an Active Constituent in Cell Biology, *Chem. Rev.*, 2008, **108**, 74–108.

5 B. C. Gibb, Hydrophobia, *Nat. Chem.*, 2010, **2**, 512–513.

6 P. Jungwirth and P. S. Cremer, Beyond Hofmeister, *Nat. Chem.*, 2014, **6**, 261–263.

7 J. W. Barnett, M. R. Sullivan, J. A. Long, D. Tang, T. Nguyen, D. Ben-Amotz, B. C. Gibb and H. S. Ashbaugh, Spontaneous Drying of Non-Polar Deep-Cavity Cavitand Pockets in Aqueous Solution, *Nat. Chem.*, 2020, **12**, 589–594.

8 B. A. Rogers, H. I. Okur, C. Yan, T. Yang, J. Heyda and P. S. Cremer, Weakly Hydrated Anions Bind to Polymers but Not Monomers in Aqueous Solutions, *Nat. Chem.*, 2022, **14**, 40–45.

9 J. Aupič, F. Lapenta, Ž. Strmšek, E. Merljak, T. Plaper and R. Jerala, Metal Ion–Regulated Assembly of Designed Modular Protein Cages, *Sci. Adv.*, 2022, **8**, eabm8243.

10 D. Ben-Amotz, Electric Buzz in a Glass of Pure Water, *Science*, 2022, **376**, 800–801.

11 A. J. Bredt, Y. Kim, D. Mendes de Oliveira, A. S. Urbina, L. V. Slipchenko and D. Ben-Amotz, Expulsion of Hydroxide Ions from Methyl Hydration Shells, *J. Phys. Chem. B*, 2022, **126**, 869–877.

12 Z. Li, C. Li, Z. Wang and G. A. Voth, What Coordinate Best Describes the Affinity of the Hydrated Excess Proton for the Air-Water Interface?, *J. Phys. Chem. B*, 2020, **124**, 5039–5046.

13 N. Agmon, H. J. Bakker, R. K. Campen, R. H. Henchman, P. Pohl, S. Roke, M. Thamer and A. Hassanali, Protons and Hydroxide Ions in Aqueous Systems, *Chem. Rev.*, 2016, **116**, 7642–7672.

14 D. Ben-Amotz and D. M. d. Oliveira, Surfactant Aggregate Size Distributions above and Below the Critical Micelle Concentration, *J. Chem. Phys.*, 2021, **155**, 224902.

15 O. A. Francisco, H. M. Glor and M. Khajehpour, Salt Effects on Hydrophobic Solvation: Is the Observed Salt Specificity the Result of Excluded Volume Effects or Water Mediated Ion-Hydrophobe Association?, *ChemPhysChem*, 2020, **21**, 484–493.

16 D. Mendes de Oliveira and D. Ben-Amotz, Spectroscopically Quantifying the Influence of Salts on Nonionic Surfactant Chemical Potentials and Micelle Formation, *J. Phys. Chem. Lett.*, 2021, **12**, 355–360.

17 P. Mukerjee, K. Mysels and P. Kapauan, Counterion Specificity in the Formation of Ionic Micelles - Size, Hydration, and Hydrophobic Bonding Effects, *J. Phys. Chem.*, 1967, **71**, 4166–4175.

18 C. M. Jäger, A. Hirsch, B. Schade, C. Böttcher and T. Clark, Counterions Control the Self-Assembly of Structurally Persistent Micelles: Theoretical Prediction and Experimental Observation of Stabilization by Sodium Ions, *Chem.–Eur. J.*, 2009, **15**, 8586–8592.

19 F. S. Lima, H. Chaimovich, I. M. Cuccovia and D. Horinek, Molecular Dynamics Shows That Ion Pairing and Counterion Anchoring Control the Properties of Triflate Micelles: A Comparison with Triflate at the Air/Water Interface, *Langmuir*, 2014, **30**, 1239–1249.

20 S. Pullanchery, S. Kulik, B. Rehl, A. Hassanali and S. Roke, Charge Transfer across C–H⋯O Hydrogen Bonds Stabilizes Oil Droplets in Water, *Science*, 2021, **374**, 1366–1370.

21 E. Poli, K. H. Jong and A. Hassanali, Charge Transfer as a Ubiquitous Mechanism in Determining the Negative Charge at Hydrophobic Interfaces, *Nat. Commun.*, 2020, **11**, 901.

22 F. A. Long and W. F. McDevit, Activity Coefficients of Nonelectrolyte Solutes in Aqueous Salt Solutions, *Chem. Rev.*, 1952, **51**, 119–169.

23 T. J. Morrison and F. Billett, The Salting-out of Non-Electrolytes. Part II. The Effect of Variation in Non-Electrolyte, *J. Chem. Soc.*, 1952, 3819–3822, DOI: **10.1039/jr9520003819**.

24 W.-H. Xie, W.-Y. Shiu and D. Mackay, A Review of the Effect of Salts on the Solubility of Organic Compounds in Seawater, *Mar. Environ. Res.*, 1997, **44**, 429–444.

25 J. E. Desnoyers, M. Billon, S. Léger, G. Perron and J.-P. Morel, Salting out of Alcohols by Alkali Halides at the Freezing Temperature, *J. Solution Chem.*, 1976, **5**, 681–691.

26 R. Aveyard and R. Heselden, Salting-out of Alkanols by Inorganic Electrolytes, *J. Chem. Soc., Faraday Trans. 1*, 1975, **71**, 312–321.

27 F. L. Wilcox and E. E. Schrier, Salt Effects in Alcohol-Water Solutions – Application of Scaled Particle Theory to Salting-out of Polar Molecules, *J. Phys. Chem.*, 1971, **75**, 3757–3764.

28 S. Weisenberger and A. Schumpe, Estimation of Gas Solubilities in Salt Solutions at Temperatures from 273 K to 363 K, *AIChE J.*, 1996, **42**, 298–300.

29 H. Katsuto, R. Okamoto, T. Sumi and K. Koga, Ion Size Dependences of the Salting-out Effect: Reversed Order of Sodium and Lithium Ions, *J. Phys. Chem. B*, 2021, **125**, 6296–6305.

30 S. Hervø-Hansen, D. Lin, K. Kasahara and N. Matubayasi, Free-Energy Decomposition of Salt Effects on the Solubilities of Small Molecules and the Role of Excluded-Volume Effects, *Chem. Sci.*, 2024, **15**(2), 477–489.

31 R. Okamoto and K. Koga, Theory of Gas Solubility and Hydrophobic Interaction in Aqueous Electrolyte Solutions, *J. Phys. Chem. B*, 2021, **125**, 12820–12831.

32 J. A. Long, B. M. Rankin and D. Ben-Amotz, Micelle Structure and Hydrophobic Hydration, *J. Am. Chem. Soc.*, 2015, **137**, 10809–10815.

33 C. M. Wentworth, R. L. Myers, P. S. Cremer and L. D. Zarzar, Investigating Oil Solubilization into Nonionic Micelles by Raman Multivariate Curve Resolution, *Aggregate*, 2023, **4**, e385.

34 P. Mukerjee and C. C. Chan, Effects of High Salt Concentrations on the Micellization of Octyl Glucoside: Salting-out of Monomers and Electrolyte Effects on the Micelle-Water Interfacial Tension, *Langmuir*, 2002, **18**, 5375–5381.